Article

Not peer-reviewed version

Development, Analytical Characterization, and Bioactivity Evaluation of *Boswellia Serrata* Extract-Layered Double Hydroxide Hybrid Composites

Stefania Cometa , Francesco Busto , Andrea Castellaneta , Andrea Cochis , Ziba Najmi , Rosanna Rizzi , Ilario Losito , Elvira De Giglio *

Posted Date: 24 July 2023

doi: 10.20944/preprints202307.1535.v1

Keywords: Boswellia Serrata extract; layered double hydroxides; composite; drug delivery system; antimicrobial; anti-inflammatory

Article

Development, Analytical Characterization, and Bioactivity Evaluation of *Boswellia Serrata* Extract-Layered Double Hydroxide Hybrid Composites

Stefania Cometa [1], Francesco Busto [2,3], Andrea Castellaneta [2], Andrea Cochis [4], Ziba Najmi [4], Rosanna Rizzi [5], Ilario Losito [2] and Elvira De Giglio [2,3,*]

[1] Jaber Innovation s.r.l., Via Calcutta 8, 00144 Rome, Italy. stefania.cometa@jaber.it (S.C.)
[2] Department of Chemistry, University of Bari, Via Orabona 4, 70126 Bari, Italy; f.busto3@studenti.uniba.it (F.B.); andrea.castellaneta@uniba.it (A.C.1); ilario.losito@uniba.it (I.L.); elvira.degiglio@uniba.it (E.D.G.)
[3] INSTM, National Consortium of Materials Science and Technology, Via G. Giusti 9, 50121 Florence, Italy.
[4] Center for Translational Research on Autoimmune and Allergic Disease, CAAD, Department of Health Sciences, Università del Piemonte Orientale UPO, 28100 Novara, Italy; andrea.cochis@med.unipo.it; (A.C.2) ziba.najmi@med.uniupo.it (Z.N.);
[5] Institute of Crystallography-CNR, Via G. Amendola, 122/o, 70126 Bari, Italy; rosanna.rizzi@ic.cnr.it (R.R.).
* Correspondence: elvira.degiglio@uniba.it.

Abstract: New hybrid composites based on the inclusion of a vegetal extract, i.e., *Boswellia Serrata* extract (BSE), rich in boswellic acids, well known as a potent anti-inflammatory natural drug, in a lamellar solid layered double hydroxide (LDH), i.e. a Magnesium Aluminum Carbonate, were developed and characterized in the present work. The adopted LDH exhibits a layered crystal structure, comprised of positively charged hydroxide layers and interlayers composed of carbonate anions and water molecules, thus it was expected to embed negatively charged boswellic acids. In the present case, a calcination process was also adopted on LDH to increase organic acids loading, based on the replacement of original inorganic anions. An accurate investigation was carried out by TGA, PXRD, FT-IR/ATR, XPS and LC-MS to ascertain the nature, interaction, and quantification of the active molecules of the vegetal extract loaded in the developed hybrid materials. As a result, a significant disruption of the original layered structure was observed in LDH subjected to calcination (LDHc), and this material was able to include a higher amount of organic acids when its composite with BSE was prepared. However, *in vitro* tests on composites bioactivity, expressed in terms of antimicrobial and anti-inflammatory activity, evidenced LDH-BSE as a better material compared to BSE and to LDHc-BSE, thus suggesting that, though the embedded organic acids amount was lower, they could be more available since not firmly bound to the clay. The composite was able to significantly decrease the number of viable pathogens such as *Escherichia Coli* and *Staphylococcus aureus,* as well as the internalization of toxic active species into human cells imposed to oxidative stress in comparison to the BSE.

Keywords: *Boswellia Serrata* extract; layered double hydroxides; composite; drug delivery system; antimicrobial; anti-inflammatory

1. Introduction

Boswellia serrata extract (BSE), an oleogum resin of Indian Frankincense, mainly employed in traditional Asiatic medicine, has recently gained growing popularity in the phytochemical-based management of a variety of inflammatory diseases (such as arthritis, osteoarthritis, inflammatory bowel disease, allergy, and asthma) [1,2]. In addition, recent studies evidenced also a potential antimicrobial activity of the extract [3,4]. The main active compounds contained in BSE are pentacyclic triterpenic acids, called boswellic acids (BAs), which are considered the main responsible for the anti-inflammatory activity of the resin. The main drawback in the use of BSE is related to its poor aqueous solubility and limited bioavailability. In this respect, different inclusion strategies have

 doi:10.20944/preprints202307.1535.v1

been proposed to enhance solubility, dissolution rate and body absorption, mainly based on the employment of phospholipids, cyclodextrins or, in general, polymer-based vehicles [5–10].

Nowadays, extensive research efforts in pharmaceutical and biopharmaceutical science have been addressed to the possibility to embed active ingredients in clays, such as lamellar host lattices, in alternative to polymeric carriers, to develop inorganic–organic hybrids [11–13]. These lamellar clays are aimed to convey the drug release in its pharmaceutical target, modify drug pharmacokinetic or release rate, for example by maintaining pharmacologically active drug levels for long periods and thus avoiding repeated administrations, or to enhance the drug bioavailability, a problem particularly frequent in the case of natural extracts, containing different lipophilic molecules, such as BSE.

In this scenario, a particularly appealing candidate for the development of these hybrid composites was represented by layered double hydroxides (LDH), which are based on positively charged brucite-like layers with divalent and trivalent cations coordinated with hydroxyl groups, balanced by the anions in the interlayer spaces [14]. These clays, present in nature, can be also easily synthesized in laboratory by means, among others, of three main synthetic preparation roots, i.e.: 1) exchange reaction, 2) direct coprecipitation and 3) hydrothermal method [15]. Regarding their toxicity, LDH were found to show minimized cytotoxic effect [16]. Moreover, LDH were already used in medicine for their antiacid and antipepsin activity [14]. Due to their interlayer cages filled with different charge-balancing anions (usually nitrate or carbonate anions), LDH can be applied to encapsulate various organic guests having anionic nature. LDH containing carbonate as interlayer anion is not particularly prone to anion-exchange but, if thermally treated, it can be decomposed into a mixed oxide and then, in this form, it can re-adsorb water and anions as it returns to its original structure. Therefore, calcined hydrotalcites can be a very interesting support material for intercalation of organic molecules [17].

In this study, we have developed for the first time an LDH-BSE inorganic-organic hybrid composite, with the aim to carry out a supramolecular structure able to enhance the anti-inflammatory and antimicrobial abilities of BSE. Different works documented the advantage in employing LDH to vehicle poorly soluble molecules [18–20]. Here we have chosen a magnesium aluminium carbonate, as received (LDH) or thermally treated by calcination at 450°C (LDHc), to embed a BSE rich in BAs. The chemical composition, in terms of abundance percentage, of the different BAs in the extract, as well as when embedded in the LDH and LDHc carriers, was investigated by means of Liquid Chromatography- Mass Spectrometry (LC-MS) analysis. The hybrid composites were analytically characterized by Fourier Transform Infrared Spectroscopy (FT-IR), Powder X-Ray Diffraction (PXRD), X-ray Photoelectron Spectroscopy (XPS) and thermogravimetric analysis (TGA). All these investigations evidenced the ability of calcined clay to embed higher BSE amount than bare LDH. On the other hand, a higher bioactivity, in terms of anti-inflammatory and antimicrobial properties, was ascribed to the hybrid based on the non-calcined LDH: indeed, a slight antimicrobial activity against *E. coli* and *S. aureus* as well as a significant decrease of toxic reactive oxygen species (ROS) internalized by human cells imposed to oxidative stress was shown by LDH-BSE composite. On the contrary, a poor response in the *in vitro* tests was exerted by LDHc-BSE and bare BSE. In this respect, this study clearly evidenced the opportunity to develop hydrotalcite based-hybrid materials able to enhance the performances of the bare natural extract.

2. Results and Discussion

2.1. Thermal analysis

Thermal properties of the inorganic-organic composites were studied by means of thermogravimetric analysis (TGA). In **Figure 1**, TG (a and c) and derivative TG traces (b and d) of LDH- and LDHc-based hybrids, as well as their feed materials, were reported.

Preprints (www.preprints.org) | NOT PEER-REVIEWED | Posted: 24 July 2023 doi:10.20944/preprints202307.1535.v1

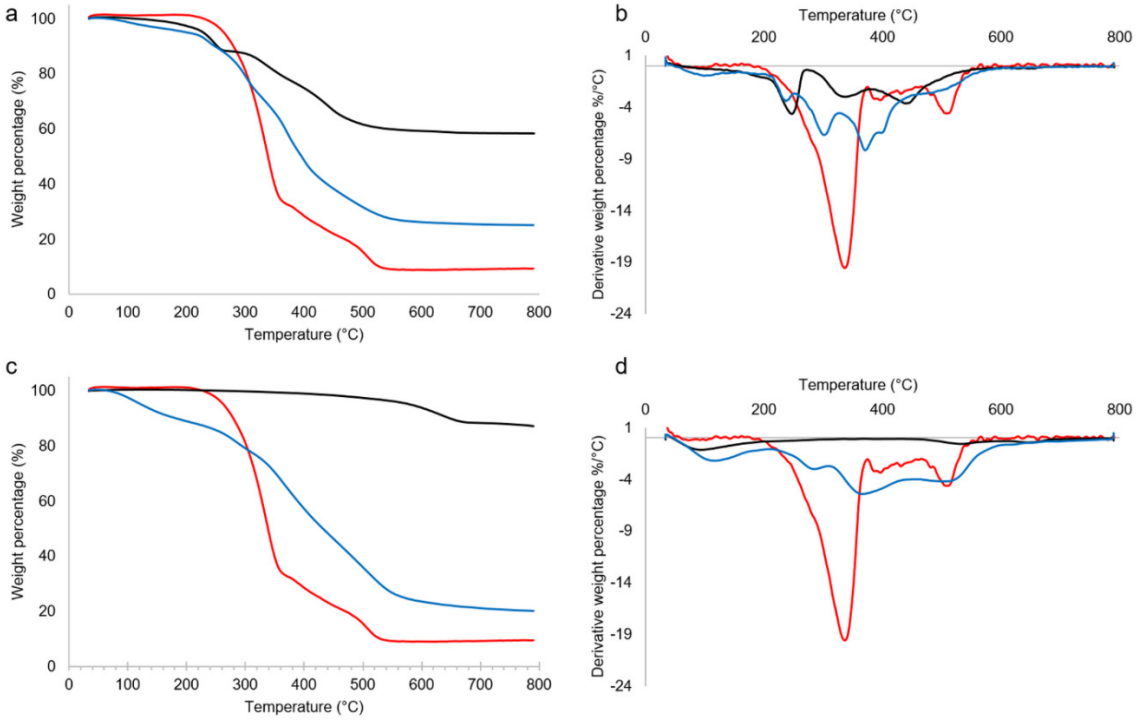

Figure 1. TG (a and c) and derivative TG (b and d) traces in the range 30-800°C in nitrogen of: a) and b) LDH (black line), BSE (red line) and LDH-BSE (blue line); c) and d) LDHc (black line), BSE (red line) and LDHc-BSE (blue line).

The TG and DTG diagrams of LDH (black line, panels a and b, respectively) showed an initial weight loss up to 180°C equal to 2%, corresponding to the desorption of surface water. The second weight loss, occurred from 180 to 270°C, was about 9% and corresponded to desorption of interlayer water, with a peak at 248°C. The third and fourth weight losses fell at 340 and 440°C (15 and 16% of weight loss, respectively), relevant to the decomposition of carbonate anions (with CO_2 evolution) and to dehydroxylation of the mixed metal oxides. Similar attributions were reported by other authors [17,21]. The residue at 800°C was equal to 58%. Stanimirova *et al.* reported that hydrotalcite thermal decomposition passed through a series of metaphases forming a mixture of MgO and $MgAl_2O_4$ as a final product of thermolysis [22].

The TG and DTG diagrams of LDHc (black line, panels c and d, respectively) showed curves totally different from those relevant to the non-calcined sample. Indeed, excluding the initial step due to surface water evolution (up to 180°C, corresponding to 5%), thermal decomposition of the calcined sample occurred at very high temperatures, *i.e.*, in the range 460-700°C, with a 7% of weight loss. The residue at 800°C was equal to 88%. These findings confirmed the occurred calcination.

BSE thermogravimetric analysis (red line, present in all the panels) showed a negligible water/volatiles content and a main thermal event occurring in the range 200-365°C, with a sharp peak at 339°C, corresponding to a 66.5% weight loss percentage, followed by several minor thermal events in the range 365-545°C, corresponding to 24.5% weight loss percentage. The residue at 800°C was equal to about 9%.

Finally, the thermogravimetric curves of the BSE-embedded LDH materials (see blue lines in **Figure 2**) revealed a multi-step decomposition pattern. Especially in the case of LDH, due to the initial complexity of TG and DTG traces relevant to the clay, a strong overlap between these mass loss events and those relevant to BSE was here observed, making any single event difficult to disentangle. At 800°C, a residue of 25 and 21% was found for LDH-BSE and LDHc-BSE specimens. These values, apparently similar, must be related to the residues of the bare LDH and LDHc samples: considering that the residue at 800°C of LDHc was significantly higher than that relevant to LDH (i.e., 88 vs 58%),

Preprints (www.preprints.org) | NOT PEER-REVIEWED | Posted: 24 July 2023 doi:10.20944/preprints202307.1535.v1

it can be hypothesized that a huge increment in BSE loading occurred in the calcined clay. This observation has been confirmed by LC-MS analysis (*vide infra*). Finally, the TGA results indicated that both LDH and LDHc embedding BSE were thermally stable up to about 200°C.

2.2. Powder X-Ray Diffraction analysis

PXRD is a powerful tool commonly used for hydrotalcite compounds to verify the expansion occurring between the hydroxide layers after the substitution of relatively small divalent anions, such as sulphate, nitrate, or carbonate with bulky molecules. This expansion serves as crucial evidence of intercalation inside the lamellar host structure.

In Figure 2 the PXRD patterns of LDH-BSE and LDHc-BSE as well as the corresponding patterns of the feed materials (*Boswellia Serrata* powder extract, LDH and LDHc) were compared. The experimental LDH pattern exhibited well-defined and characteristic peaks, that can be indexed by a hexagonal lattice with R-3m rhombohedral symmetry, which is commonly used to describe the LDH structures [23]. In addition, the two strongest and most characteristic low-angle reflections, 003 and 006, were observed approximately at 11.6° (2ϑ) (d = 7.6 Å) and 23.4° (2ϑ) (d=3.8 Å), respectively, with values closely aligned with the reference pattern for the carbonated LDH phase, thus indicating a well-crystallized sample.

In the LDH structure, the unit cell parameters, a and c, represent the average distance between two metal ions in the layers and three times the distance from the centre of one layer to the next, respectively. The value of a (=2d110) depends on the average radii of the metal cations, while the value of c (=3d003) depends on their average charge, the nature of the interlayer anion, and the water content [24,25].

In contrast, LDHc exhibited a significantly different pattern, where the peaks corresponding to 003 and 006 reflections disappeared, indicating a complete destruction of the layered structure of the original hydrotalcite.

When LDHc is exposed to the BSE, it partially reacquires the original layered structure, as shown in Figure 2. The LDH structure, even when calcined, can accommodate different types of anions/molecules and, due to the different sizes of the counterions, variations in the lattice parameters are expected, resulting in peak positions shift [26].

In our study, the PXRD patterns of the resulting products (LDH-BSE and LDHc-BSE) retained the major characteristic features of the corresponding LDH and LDHc, with no shift of the peaks towards lower angles. The unaltered basal spacing (d003) clearly indicated that the intercalation of BSE acid anions within the lamellar host structure did not occur in the composite organic-inorganic derivatives.

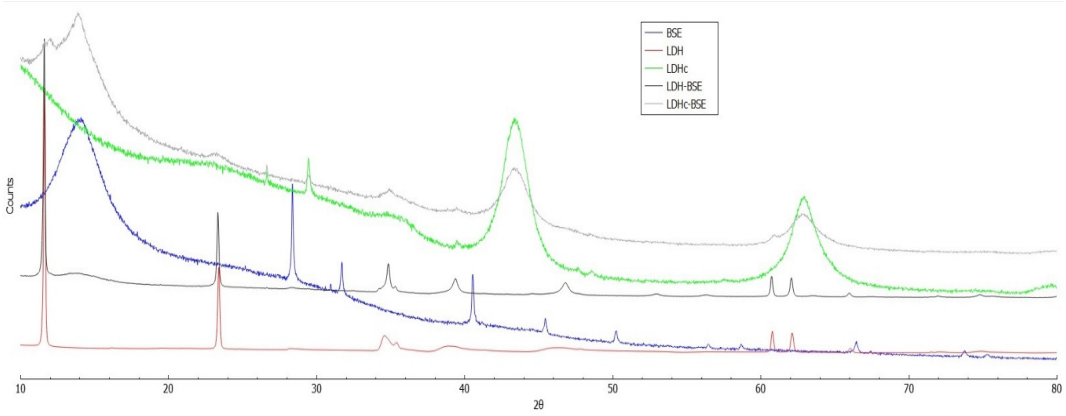

Figure 2. From top to bottom, the powder X-ray diffraction patterns of LDHc-BSE; LDHc; BSE; LDH-BSE and LDH.

Preprints (www.preprints.org) | NOT PEER-REVIEWED | Posted: 24 July 2023 doi:10.20944/preprints202307.1535.v1

2.3. Bulk and surface investigations

FT-IR/ATR analysis was carried out on the hybrid composites as well as on their feed materials to highlight possible organic-inorganic moieties interactions. In **Figure 3**, ATR spectra of LDH, BSE and LDH-BSE (panel a) and LDHc, BSE and LDHc-BSE (panel b) are reported.

As far as the pristine LDH sample, a broad band at about 3419 cm^{-1} was due to the stretching of hydroxyl groups of water and hydroxyl groups located between the layers [27], while the peak at 1366 cm^{-1} could be attributed to carbonate [17]. The other peaks under 800 cm^{-1} could be assigned to metal-oxygen and metal hydroxide stretching modes.

The ATR spectrum of BSE revealed the presence of absorption bands at 3423 cm^{-1} (OH stretching), 2924 cm^{-1} (C-H stretching), 1699 cm^{-1} (C=O stretching of aryl acid), 1454 cm^{-1} (C=C bending), and 1241 cm^{-1}(C=C-C=O stretching of aryl ketone) [8].

No changes in LDH-BSE ATR spectrum were observed respect to those of the starting materials. Indeed, the spectrum appears as a superimposition of LDH and BSE spectra, thus suggesting a simple BSE absorption on the clay.

In the LDHc sample, the –OH stretching band intensity significantly decreased after calcination, due to the water and interlayer hydroxyl groups loss caused by calcination. In the wavenumber range 1500-1300 cm^{-1}, peaks assigned to residual interlayer CO_3^{2-} anion were detected, as reported by Mališová and coworkers, who found a total peak disappearance at calcination temperatures higher than 550°C [28]. The same authors stated that in the calcination process, overheating must be absolutely avoided, since it could lead to a spinel structure resistant to rehydration, thus not allowing the reconstruction of a hydrotalcite-like structure where the anions of interest can be hosted. In this respect, the calcination temperature chosen in this work was maintained at 450°C.

Finally, the LDHc-BSE spectrum showed a decrease of the vibration band at 1699 cm^{-1} due to the C=O bond present in the carboxyl group of BAs, in addition to the appearance of the bands at 1549 and 1379 cm^{-1} due to asymmetric and symmetric stretching vibration of carboxylates. This means that part of BAs was stored in LDH in their ionic form and probably established ionic interactions with the clay, which in turn could explain the partial BAs extraction by methanol evidenced in the LC-MS studies (*vide infra*).

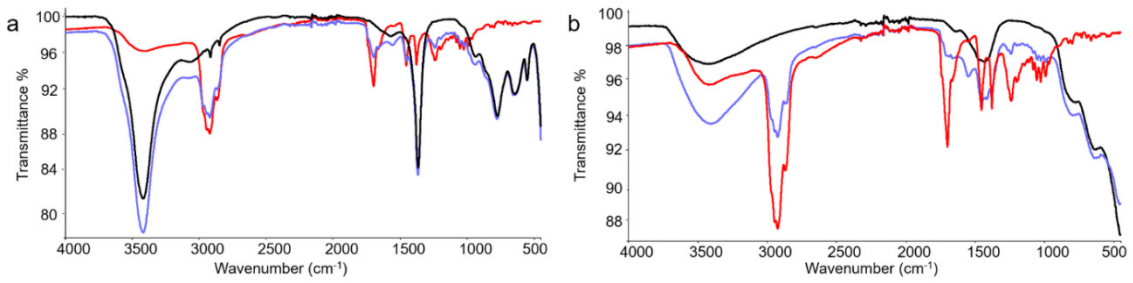

Figure 3. FT-IR/ATR spectra of a) LDH (black line), BSE (red line) and LDH-BSE (blue line) and b) LDHc (black line), BSE (red line) and LDHc-BSE (blue line).

XPS analysis was carried out to obtain information on the surface composition of the developed hybrid composites and to highlight possible clay/active principles interactions. In **Table 1**, the surface composition of the composites, as well as the feed materials, have been reported.

Table 1. Surface composition by XPS analysis of BSE, hydrotalcites and BSE-embedded hydrotalcites.

Sample	Atomic %						
	C1s	O1s	Ca2p	Na1s	Al2p	Mg1s	Si2p
BSE	86.1	12.6	0.9	0.4	--	--	--

Preprints (www.preprints.org) | NOT PEER-REVIEWED | Posted: 24 July 2023 doi:10.20944/preprints202307.1535.v1

LDH	47.4	42.3	--	--	5.2	3.7	1.5
LDH-BSE	76.4	19,1	--	--	1.5	1.0	2.1
LDHc	16.8	55.2	--	--	11.2	16.8	0.7
LDHc-BSE	79.1	16.7	--	--	1.6	1.3	1.2

It can be observed that the surface composition of the hydrotalcite-based materials, in terms of Mg/Al ratio, does not reflect the stoichiometric one, typical of MgAl carbonate clays. This phenomenon is not surprising, since the chemistry of the surfaces often differs from the bulk [29]. Indeed, an Mg/Al ratio equal to 0.7:1, 0.7:1, 1.4:1 and 0.8:1 was recorded for LDH, LDH-BSE, LDHc and LDHc-BSE, respectively. Another important finding was the decreased carbon amount after the calcination process; on the other hand, a significant increase in C1s atomic percentage was detected after BSE embedding, both on pure and calcined hydrotalcite. Considering, for example, the C1s/Al2p ratio, this ratio changed from 1.5:1 to 49:1 when LDHc was loaded with BSE (*i.e.*, about 33 times higher) and from 9:1 to 51:1 in the case of the LDH-based system (*i.e.*, about 6 times higher). Therefore, a higher BSE surface amount was clearly detected on LDHc-BSE.

For a deeper investigation of the developed hybrid composites, deconvolution of the high-resolution C1s spectra has been performed (see **Figure 4**).

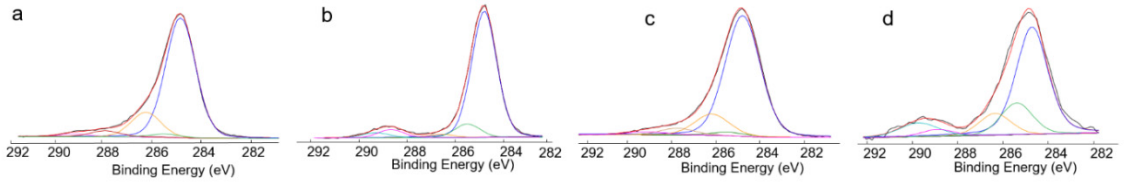

f

Sample	Atomic percentage (%)					
	CHx (284.8 eV)	C-COOR (285.5.eV)	C-OR (286.4 eV)	C=O, O-C-O (287.8 eV)	COOR (289.0 eV)	Carbonate (289.5 eV)
BSE	78.3	2.0	15.8	3.9	2.0	--
LDHs	80.8	8.6	2.0	--	5.2	3.5
LDHs-BSE	77.8	2.4	13.7	4.3	2.1	--
$LDHs_{calc}$	60.1	16.5	11.4	--	3.5	8.6
$LDHs_{calc}$-BSE	78.6	8.2	8.6	2.4	2.2	--

Figure 4. C1s curve-fitting of: a) BSE, b) LDH, c) LDH-BSE, d) LDHc and e) LDHc-BSE samples. In panel f), the peaks attributions and atomic percentages were reported. Uncertainty in binding energy values was ± 0.2 eV.

BSE C1s spectrum (**Figure 4a**) clearly evidenced a predominance of C-C or C=C bonds, coded as CHx, as expected by the chemical structure of boswellic acids. However, since this contribution was affected by hydrocarbon contamination, always present in XPS analyses, it cannot be considered as an indication of BSE presence on the surface of the hybrid materials. Other peaks, relevant to oxygenated functionalities, proper of most of compounds of natural origin, can be observed. Carboxylic acid groups, ascribable to boswellic acids and/or other BSE components, have been detected.

In LDH and LDHc C1s spectra (Figure 4b and d) a carbonate peak was detected at the highest binding energies. Even if the absolute value of carbonate percentage was higher in LDHc than in LDH sample (see Figure 4f), the carbonate presence in the calcined clay was significantly lower. Indeed, considering the carbonate/Al2p ratio, it was 1:3 in LDH and 1:10 in LDHc sample, evidencing a partial carbonate removal, as observed also by FT-IR and TGA analyses.

Finally, C1s spectra of both LDH-BSE and LDHc-BSE samples (Figure 4c and e) showed the absence of carbonate peaks. This finding could be related to a total surface coverage by the plant extract in both composites, rather than to partial or total replacement of the carbonate by boswellic acids. Indeed, PXRD analysis allowed us to exclude the latter hypothesis. On the other hand, as

Preprints (www.preprints.org) | NOT PEER-REVIEWED | Posted: 24 July 2023 doi:10.20944/preprints202307.1535.v1

evidenced by LC-MS analysis (*vide infra*), while methanol extraction totally removed BSE from LDH, a partial BSE removal was observed for the LDHc-BSE sample, suggesting a strong interaction between the extract compounds and the calcined clay, although an intercalation cannot be invoked.

To shed light on the interaction occurring between LDHc and the BSE compounds not removed by solvent extraction, a deeper investigation on the LDHc-BSE sample after two methanol extractions has been performed. Both FT-IR and XPS spectra, reported in Figure 5, suggested that the part of BSE firmly adsorbed on the calcined clay could be ascribed to BAs in their anionic form, which could be electrostatically bound with positively charged lamellae of LHDc. Indeed, the C=O stretching of COOH totally disappeared after methanol extraction, as shown by FTIR analysis (Figure 3a), while a shift in COOR peak at lower binding energies (288.6 eV, typical of COO^- groups) was observed by XPS, together with a resurfacing of the carbonate contribution already present in LDHc (see panels b and c).

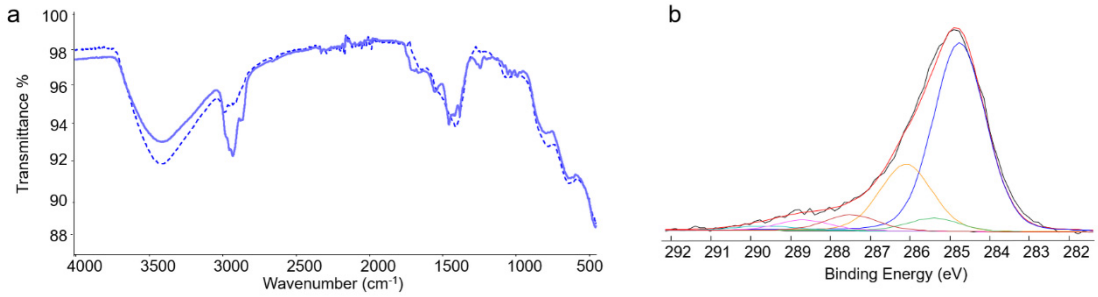

c

Sample	Atomic percentage (%)					
	CHx (284.8 eV)	C-COOR (285.5.eV)	C-OR (286.4 eV)	C=O, O-C-O (287.8 eV)	COO^- (288.6 eV)	Carbonate (289.5 eV)
HTCc-BSE after methanol extraction	62.8	4.3	22.1	5.3	3.6	1.9

Figure 5. LDHc-BSE (solid line) and LDHc-BSE after methanol extraction (dashed line) FT-IR/ATR spectra (a); XPS C1s curve fitting of LDHc-BSE after methanol extraction (b), with the relevant peaks attributions and atomic percentages (c). Uncertainty on binding energy values was ± 0.2 eV.

2.4. Targeted RPLC-ESI(-)-FTMS characterization of boswellic acids in BSE and LDH(c)-BSE hybrid composites

α-boswellic acid (α-BA) and β-boswellic acid (β-BA), along with their acetylated and oxidized forms, namely 3-acetyl α-boswellic acid (α-ABA), 3-acetyl β-boswellic acid (β-ABA), 11-keto-β-boswellic acid (β-KBA) and 3-acetyl 11-keto-β-boswellic acid (β-AKBA), have been identified as the major bioactive compounds in BSE [30–32]. As can be inferred from the chemical structures shown in **Figure S1**, the acidic properties of boswellic acids (BA) are related to the presence of a common carboxylic acid moiety. Thus, the electrospray ionization (ESI) could be recognized as a suitable *soft* ionization approach for the mass spectrometric characterization of these analytes as negative ions ($[M-H]^-$). Furthermore, the high-resolution/accuracy of the Orbitrap® mass analyser allowed the use of a very narrow (5 ppm) *m/z* extraction window to isolate the contributions of each BA $[M-H]^-$ ion from the total ion current chromatogram (TICC). The resulting extracted ion chromatograms (EIC) are shown in **Figure S2**. Notably, up to 9 peaks were observed in the EIC trace pertaining to α-BA and β-BA $[M-H]^-$ ions (*m/z* 455.3531), thus indicating the presence of multiple isomeric species (see **Figure S2A**). The unambiguous identification of α-BA and β-BA peaks was based on the comparison of the high-resolution (HR) higher energy collision dissociation (HCD) MS/MS spectra (data not shown) and retention times (see **Figure S2B**) with those obtained for their commercial analytical standards. The mass spectrometric characterization of the remaining isomers will be the object of a future work.

Similarly to what observed for α-BA and β-BA, the EIC of α-ABA and β-ABA $[M-H]^-$ ions (*m/z* 497.3636) exhibited more than just two peaks (see **Figure S2C**). All the HRMS/MS spectra of the ions responsible for these signals were characterized by the presence of a peak at *m/z* 59.0138, that is

Preprints (www.preprints.org) | NOT PEER-REVIEWED | Posted: 24 July 2023 doi:10.20944/preprints202307.1535.v1

compatible with the detachment of the acetate ion (CH_3COO^-) from acetylated ion species. Notably, the signal at *m*/*z* 59.0138 was the only observed peak in the HRMS/MS spectra pertaining to the last two eluting species shown in **Figure S2C**. As shown in **Scheme S1**, the formation of the acetate ion as the dominant fragmentation pathway can be rationalized in the case of α-ABA and β-ABA. Here, a β-lactone is formed after the nucleophilic attack of the carboxylate group at its β position, while the acetate ion is released as the leaving group.

Both α-BA and β-BA and their acetylated form have been detected in the oleogum resin of several Boswellia species, including Boswellia Serrata [33,34]. Schmiech et al. [33] proposed a valuable chromatographic approach for the separation of α-BA, β-BA, α-ABA, and β-ABA. As expected, the acetylation enhanced the retention on a C18 stationary phase, but more importantly, a similar retention time (RT) shift was observed among the corresponding non acetylated and acetylated species. Our chromatographic approach was inspired by the work of Schmiech et al. [33] (see **Section 3.3.4**). Interestingly, a similar RT shift (about 3.4 min) was observed for the chromatographic peaks pertaining to α-BA, β-BA and for those that have been putatively attributed to α-ABA, and β-ABA in **Figure S2C.**

A single peak was observed in the EIC trace pertaining to β-AKBA (*m*/*z* 511.3429) (see **Figure S2E**), while an intense peak, followed by a low intensity signal (labelled as **1d** in **Figure S2D**) was observed in the EIC trace related to β-KBA (*m*/*z* 469.3323). Interestingly, the $[M-H]^-$ ions that were responsible for the latter two peaks exhibited very similar HCD-HRMS/MS spectra (data not shown). These might be attributed to β-KBA and α-KBA. The most intense and early eluting peak in **Figure S2D** has been attributed to β-KBA, that it is expected to be dominant in BSE [35]. Moreover, Schmiech *et al.* reported a higher retention of α-KBA in respect to β-KBA when the two analytes were subjected to a RPLC separation on a pentafluorophenyl (PFP) stationary phase [35].

The tentative identification β-KBA and β-AKBA was also supported by the UV-Vis characterization of BSE. Asteggiano *et al*. [36] developed an RPLC-UV method for the characterization of several boswellic acids (BA). Here, 250 nm was adopted as the diagnostic absorption wavelength for β-KBA and β-AKBA. Interestingly, a perfect alignment was observed between the peaks that have been putatively attributed to β-KBA and β-AKBA (see **Figure S2D** and **E**), and those that were observed in the RPLC-UV chromatogram recorded at 250 nm (**Figure S2F**).

In this study, the hyphenation of reversed-phase liquid chromatography and high-resolution mass spectrometry was exploited to quantitatively assess the loading of BA and their isomers in LDH-BSE and LDHc-BSE hybrid composites. We focused on α-BA, β-BA, and those species that were tentatively identified as α-ABA, β-ABA, β-KBA, and β-AKBA. We also considered all the isomers exhibiting significantly intense peaks in the EIC traces shown in **Figure S2A** and **C**. We will refer to these species using the following nomenclature, that is related to the labels adopted in **Figure S2A** and **C**: BA isomer 3 (peak **3a**), BA isomer 4 (peak **4a**), BA isomer 5 (peak **5a**), BA isomer 6 (peak **6a**), BA isomer 7 (peak **7a**), ABA isomer 1 (peak **1c**), ABA isomer 2 (peak **2c**), ABA isomer 3 (peak **3c**), and ABA isomer 4 (peak **4c**).

For each of the analytes of interest a calibration curve was obtained by plotting the EIC peak area calculated for each of the serial dilutions performed starting from a 100 μg/mL methanolic solution of lyophilized BSE (see **Section 3.3.6**). The mathematical equations of the calibration curves are shown in and **Table S1**. As stated in **Section 3.3.6**, the outcome of the interpolation of the normalized peak area response with the calibration curve is to be interpreted as the percentage amount of the loaded analyte into a given mass of LDH/LDHc-BSE composite, in respect to the content of such analyte in the same mass of BSE. The results are shown in **Table S2A** and graphically summarized in **Figure 6A**.

Preprints (www.preprints.org) | NOT PEER-REVIEWED | Posted: 24 July 2023 doi:10.20944/preprints202307.1535.v1

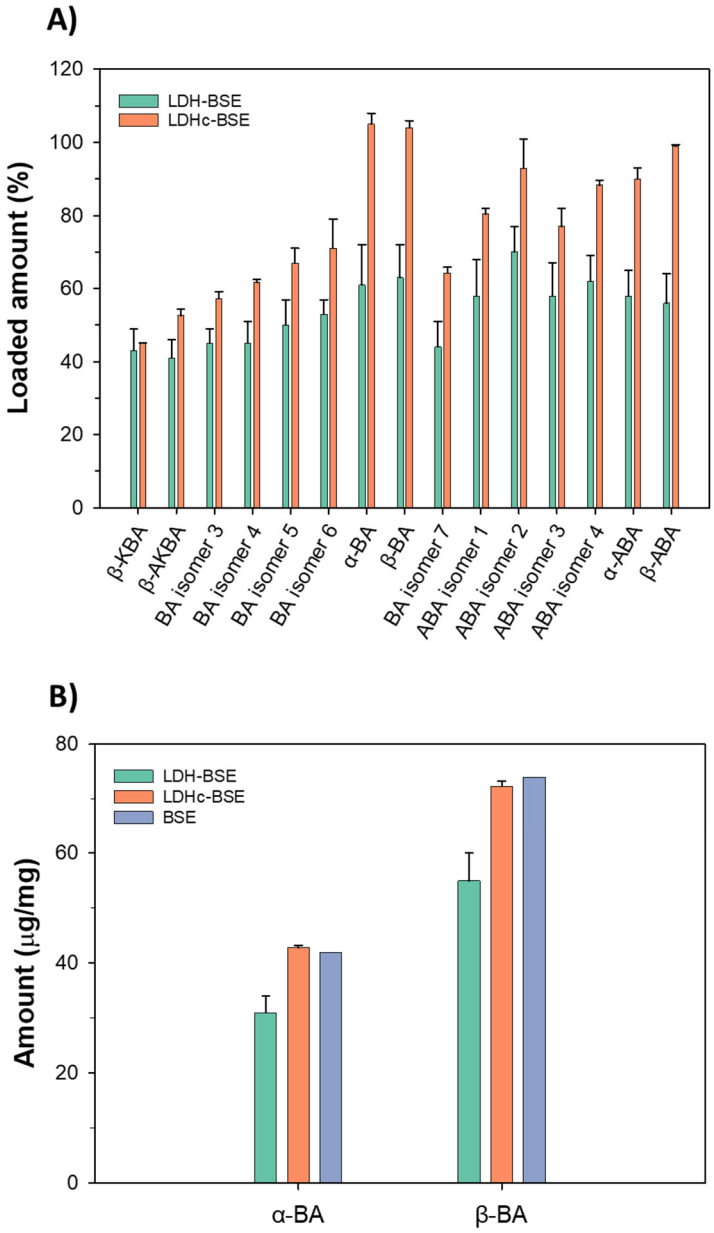

Figure 6. (A) Bar charts showing the % loaded amount of boswellic acids and their isomers in LDH/LDHc-BSE composites. For each analyte, the 100% is assumed to be corresponding to the content embedded in an equal mass of BSE. Here, bar heights are representative for the mean values calculated for three extraction replicates (see **Section 3.3.5**). The error bars are indicative of the calculated standard deviation. (B) Bar charts showing the calculated amount (μg/mg) of α-BA and β-BA embedded in BSE (blue bars), LDH-BSE (green bars), and calcinated LDH-BSE (orange bars). The bar heights are representative for the mean values calculated for three extraction replicates (see **Section 3.3.5**) in the case of LDH/LDHc composites. The error bars are indicative of the calculated standard deviation.

The loaded amount of the analytes of interest was found to be remarkably higher in LDHc-BSE than in LDH-BSE composites, except for the early eluting (*i.e.*, more polar) species, namely β-KBA and β-AKBA. This is consistent with the improved BSE loading capability of the LDHc system that was assessed by the thermal analysis (see **Section 2.1**).

Notably, the highest loading discrepancies between the two systems were observed for α-BA, β-BA and their acetylated forms (α-ABA, β-ABA). To further support these findings, we quantified the

absolute amount of α-BA, β-BA (see **Section 3.3.6**) in the inorganic-organic composites and compared the outcomes with the estimated amount in BSE. The results are shown in **Table S2B** and graphically summarized in **Figure 6B**. The mathematical equations of the calibration curves are shown in **Table S1B**. Consistently to what shown in **Figure 6A**, the estimated amount of α-BA and β-BA in the LDHc-BSE system was comparable with the one observed for pure BSE. Conversely, a lower amount was observed in LDH-BSE composites.

2.5. Antimicrobial activity of BSE-based composites

The increasing ability of bacteria to develop defence mechanisms against the biological activity of the conventional antibiotics, open for the urgent need of alternative active principles being able to counteract pathogens infections. Natural compounds and their extracts are known to hold intrinsic antibacterial activity, as well as they normally present low side effects due to their natural origin. Among the large class of such natural extracts, *Boswellia serrata* (BSE) represents an interesting source of antibacterial active compounds. It has been previously reported in the literature that this extract is largely composed of terpene substances that are known being able to bind to the membrane thus causing the formation of irreversible pores, as well as they can lower proteins synthesis, reducing ATP consumption and interfering with the quorum sensing signalling during biofilm formation [37].

Beyond these promising intrinsic antibacterial properties, it is also well known that the bioactivity of natural compounds and their extracts is limited by their chemical instability and poor aqueous solubility, which severely limit their effectiveness [38]. To overcome this limit, the composites here developed were aimed to stabilize the bioactivity of the BSE extract in solution to improve its efficacy when a bacterial infection is ongoing as a potential alternative to conventional antibiotics. Accordingly, the composites have been in direct contact for 24 hours with viable colonies of *Escherichia coli (E. coli, Gram -), Pseudomonas aeruginosa (P. aeruginosa, Gram -), Staphylococcus aureus (S. aureus, Gram +), Staphylococcus epidermidis (S. epidermidis, Gram +)* cultivated in their liquid broth media. Bacteria have been cultivated at high density ($1x10^5$ bacteria/mL) to resemble a pathological scenario and the results of the composites (LDH-BSE and LDHc-BSE) have been compared to the bare extract (BSE) to verify if they introduce an improvement in terms of antibacterial activity.

Results are reported in **Table 2** In general, LDH-BSE reported the lowest number of viable bacteria for all the tested strains in comparison to the bare extract (BSE). In particular, results were statistically significant ($p<0.05$, indicated by § in the Table 2) for *E. coli* and *S. aureus*, where the reduction of the number of viable colonies was of 63% and 34%, respectively. For other strains (*P. aeruginosa* and *S. epidermidis*) a reduction of 20% and 26% was observed too, but results were not statistically significant ($p>0.05$). Differently, LDHc-BSE showed significant results in comparison to the bare extract (BSE) only for *E. coli* ($p<0.05$, indicated by §), whereas a non-significant reduction of viable colonies was reported for *P. aeruginosa, S. aureus* and *S. epidermidis*. However, in terms of bioactivity, the difference observed between LDH-BSE and LDHc-BSE could be ascribed to the stronger interaction between the extract and the calcined clay as previously observed by the LC-MS results. Finally, as might be expected considering that the antibacterial active ingredient is related to the boswellic acids present in the extract, the composites not loaded with the extract (LDH and LDHc) showed no inhibitory activity compared to the extract per se.

To rank the obtained results, only a very limited literature can be found. In particular, Bi et al. reported similar findings showing the possibility to enhance BSE bioactivity by loading the extract into hydroxyapatite carboxymethyl cellulose composites (named HAP/BE/CMC) [39]. The antibacterial assay results demonstrated that the HAP/BE/CMC composites were able to significantly reduce the propagation of *Bacillus cereus* and *Pseudomonas aeruginosa* by the agar diffusion test in comparison to the unloaded hydroxyapatite. In the context of food packaging, Narasagoudr et al. demonstrated that the incorporation of BSE into chitosan poly (vinyl alcohol) films was significantly more effective than the BSE alone to reduce the infection of *Escherichia coli, Staphylococcus aureus and Candida albicans* [40] by the agar diffusion assay. Therefore, our results seem to be in line with previous literature suggesting for a higher bioactivity of the BSE loaded into delivery systems and it can be speculated that in particular the composite LDH-BSE represents a promising candidate for

 doi:10.20944/preprints202307.1535.v1

further investigations due to its higher bioactivity towards both Gram – and Gram + strains in comparison to the bare extract.

Table 2. Colonies Forming Unit (CFU) count of viable bacteria after being in direct contact with composites for 24 hours. Results are reported as means ± dev.st x10^7; §=p<0.05 vs BSE. Experiments were performed using six replicates.

	E. coli	*P. aeruginosa*	*S. aureus*	*S. epidermidis*
BSE	124 (± 5)	15 (± 3)	18 (± 3)	15 (± 10)
LDH	150 (± 1)	15 (± 4)	20 (± 1)	18 (± 3)
LDH-BSE	46 (± 2)§	12 (± 3)	12 (± 3)§	11 (± 1)
LDHc	120 (± 1)	16 (± 8)	17 (± 6)	29 (± 3)
LDHc-BSE	68 (± 2)§	12 (± 1)	15 (± 1)	20 (± 3)

2.6. Antinflammatory activity of BSE-based composites

To further verify the superior bioactivity of the composites in comparison to the extract, the anti-inflammatory properties were tested. Boswellic acids have been largely reported in literature to be able to interfere with many pathways involved in the inflammatory cascade such as 5-lipoxygenase, human leukocyte elastase, toposiomerase I and II, as well as Ca^{2+} and MAPK signalling in various blood cells [41]. A specific role of boswellic acids has been also clarified regarding antioxidant properties as they are involved in the inhibition of the pro-inflammatory NF-κB activator and in the modulation of other relevant inflammatory molecular targets such as AP-1 and β-catenin as well as enzymes like COX-2 and pro-inflammatory cytokines (TNF-α, IL-1β) [42]. Accordingly, a pro-inflammatory condition was induced by oxidative stress chemically generated by hydrogen peroxide addition into the culture medium; afterwards, supernatants were collected and used to cultivate cells as previously reported by the Authors [43–45]. In such pro-inflammatory scenario, the well-known scavenger ability of the boswellic acids [46,47] was expected to significantly reduce the amount of the cytotoxic oxygen- and nitrogen-derived (ROS) active species, thus protecting cells from intracellular accumulation.

Results are reported in **Figure 7.** The first interesting evidence is related to the comparable RFU values reported by the controls (cells cultivated in polystyrene - POLY) and BSE, shown in Figure 7a (not significant, p>0.05); such result confirmed the poor bioactivity of the extract per se when applied in a liquid environment due to the poor solubility, which prevented the scavenger activity towards the generated ROS. Similarly, the unloaded clays (i.e., LDH and LDHc) did not displayed any efficacy in reducing the amount of free ROS (Figure 7a, p>0.05) in comparison with controls. Conversely, LDH-BSE and LDHc-BSE composites determined a reduction of the intracellular amount of ROS, thus demonstrating the bioactivity of the BSE delivered by the hydrotalcite carrier; fluorescent images (Figure 7b) clearly demonstrated the difference in terms of intracellular ROS amount (stained in red) between the unloaded (LDH and LDHc) and BSE loaded (LDH-BSE and LDHc-BSE) systems. In particular, The LDH-BSE reported a significant reduction of the ROS in comparison to BSE (Fig. 7a, p<0.05 indicated by §) thus demonstrating the ability of the composite to increase the bioactivity of BSE. However, results were not significant when the LDHc-BSE was compared to BSE (p>0.05), thus confirming the observations made above for the antibacterial assay in relation to the lower ability of these composites to deliver the loaded BSE in comparison to the LDH-BSE ones. These results are in line with the work published by Mehta *et al.* [9]; by loading boswellic acid into a proniosomal gel for topic applications, they observed a significantly reduce of paw edema in rats induced by pharmacological administration of pro-inflammatory carrageenan. The observed effect was correlated by the Authors to the ability of the BSE to reduce in situ the cells' adsorption of toxic compounds due to oxidative stress, thus strongly reducing the activation of the pro-inflammatory cascade.

Therefore, in accordance with the antibacterial assay results, it can be speculated that the LDH-BSE composite represent a promising system for delivering and enhancing BSE bioactivity.

Preprints (www.preprints.org) | NOT PEER-REVIEWED | Posted: 24 July 2023 doi:10.20944/preprints202307.1535.v1

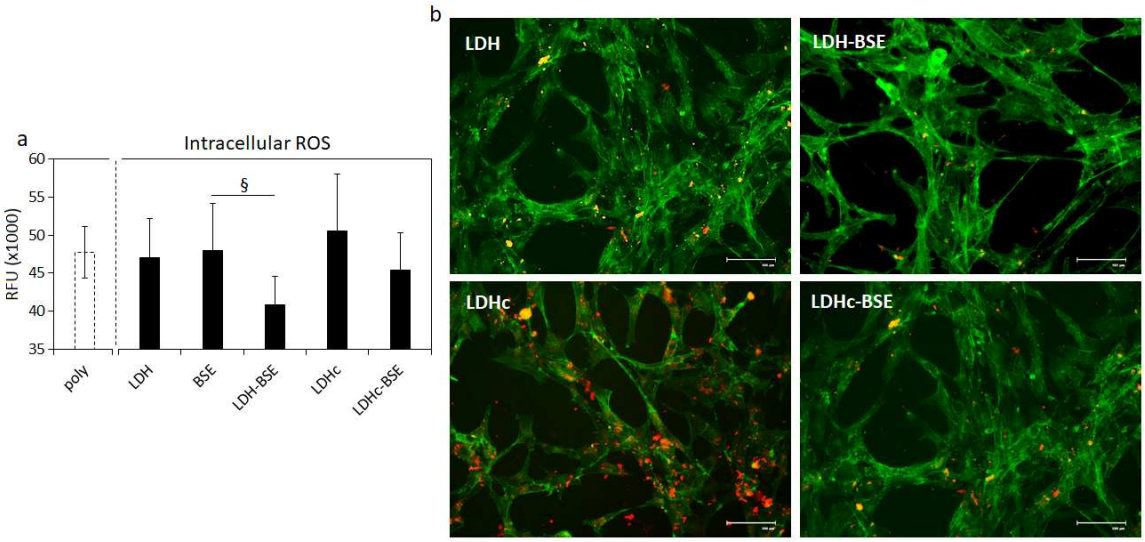

Figure 7. ROS Intracellular accumulation. (a) The quantification of the RFU due to ROS intracellular accumulation reveled that the LDH-BSE was significantly more efficient in comparison to BSE in reducing the internalization of toxic species ($p<0.05$, indicated by §); (b) in general, fluorescent images demonstrated that the BSE delivered by the composites reduced the amount of internalized toxic species suggesting for an improved bioactivity. Bars represent means±dev.st of six replicates. Images bar scale = 100 µm, ROS are stained in red, cells' cytoskeleton is stained in green.

3. Materials and Methods

3.1. Materials

Hydrotalcite synthetic (magnesium aluminum hydroxycarbonate, CAS 11097-59-9, molecular weight 603.98 g/mol), coded as LDH, has been purchased from Sigma-Aldrich (Merck, Milan, Italy). *Boswellia Serrata* powder extract (containing 65% boswellic acids, CAS 97952-72-2), coded as BSE, was purchased from Farmalabor S.p.A. (Apulia, Italy). All solvents and reagents have been purchased from Sigma Aldrich (Merck, Milan, Italy), unless otherwise specified.

3.2. Preparation of the hybrid composites based on LDH and calcined LDH

The loading of BSE was achieved by equilibrating LDH with a 0.05 M water/ethanol (25/75 v/v) solution, (considering a theoretical milliequivalents ratio between organic anions and CO_3^{2-} 2.5:1) for 24 hours at room temperature. The recovered solid, obtained by filtration, was washed three times with distilled water and then dried at 60°C until a constant weight was reached. It was expected that for LDH in their "as received" carbonate form, a minimal or no anion exchange could occur, since carbonate is preferentially sorbed and prevents further significant anion exchange. In this respect, only a surface adsorption process of BSE was expected to occur. On the other hand, carbonate can be removed by thermal decomposition, evolving carbon dioxide, by heating the hydrotalcite at temperatures higher than 400°C, as reported by Miyata [48]. Therefore, a calcination process was performed on LDH, by heating at 450°C for 2 hours [49]. The recovered solid (coded as LDHc) was then loaded using the same amount of BSE used for the non-calcined clay but replacing water with CO_2-free deionized water. Both LDH-BSE and LDHc-BSE samples were stored in a desiccator until use.

3.3. Physical-chemical characterization of the hybrid composites

3.3.1. Thermo-Gravimetric Analysis (TGA)

The thermal behavior of the hybrid composites was assessed by a PerkinElmer TGA-400 instrument (Perkin Elmer, Milan, Italy), heating 5-10 mg of the samples between 30 and 600°C. The

 doi:10.20944/preprints202307.1535.v1

analyses were performed in nitrogen, with a gas flow set at 20°C/min. Data were recorded by means of the TGA Pyris software.

3.3.2. Powder X-Ray Diffraction (PXRD) measurements

For Powder X-Ray Diffraction (PXRD) data analysis, the patterns were collected by using a Rigaku Rint2500 laboratory diffractometer with a rotating Cu anode. The instrument operated at 50 kV and 200 mA in Debye-Scherrer geometry. The diffractometer is equipped with an asymmetric Johansson Ge (111) crystal to select the monochromatic CuKα_1 radiation (λ = 1.54056 Å) along with the silicon strip Rigaku D/teX Ultra detector. The data were collected in the range of 5 to 100° (2ϑ) with a step size of 0.02° (2ϑ) and a counting time of 6 s/step. To perform the measurements, each powder sample was introduced in a glass capillary with a diameter of 0.5 mm and mounted on the goniometer's axis. The capillary was rotated during the measurement to enhance the randomization of the individual crystallites' orientations and minimize the potential impact of preferred orientation.

3.3.3. Bulk and Surface Chemical Characterization

FT-IR/ATR analyses using a Spectrum Two-PE instrument endowed with a universal ATR accessory (UATR, Single Reflection Diamond/ZnSe) supplied by PerkinElmer. For each of the relevant samples, FT-IR/ATR spectra were recorded from 400 to 4000 cm^{-1} with a 4 cm^{-1} resolution.

XPS analyses were performed using a scanning microprobe PHI 5000 VersaProbe II purchased from Physical Electronics (Chanhassen, MN). The instrument is equipped with a micro-focused monochromatized AlKα X-ray radiation source. The samples were examined in HP mode with an X-ray take-off angle of 45° (instrument base pressure ~10^{-9} mbar). The size of the scanned area was about 1400 × 200 μm. Wide scans and high-resolution spectra were recorded in FAT mode for each sample, setting pass-energy values equal to 117.4 eV and 29.35 eV, respectively. To fit the high-resolution spectra, the commercial MultiPak software version 9.9.0.8 was used. Adventitious carbon C1s were set as the reference charge (284.8 eV).

3.3.4. RPLC-ESI-FTMS instrumentation and operating conditions

The RPLC-ESI(-)-FTMS analysis was performed using a LC-MS platform implementing an Ultimate 3000 HPLC quaternary chromatographic system and a Q Exactive high-resolution quadrupole-Orbitrap mass spectrometer (Thermo Fisher, West Palm Beach, CA, USA). Here, the chromatographic column effluent was transferred into the Heated ElectroSpray Ionization (HESI) interface (Thermo Fisher, West Palm Beach, CA, USA) mounted on the mass spectrometer. The RPLC separations of BA and their isomers were performed using a C18 Ascentis Express column (15 cm length, 2.1 mm internal diameter) packed with core-shell 2.7 μm particles (Supelco, Bellefonte, PA, USA) and operated at a 0.2 mL/min flow. A 5 μL sample volume of the resulting solution was subjected to RPLC-ESI(-)-FTMS/MS analysis.

The separation of BA and their isomers was obtained using a modified version of the chromatographic approach proposed by Schmiech *et al.* [33]. The following multi-step binary elution gradient, based on a 80:20 v/v methanol/water mixture as phase A and methanol as phase B, both containing a 2.5 mM nominal concentration of ammonium acetate and ammonia, was adopted: 0-2 min) isocratic at 10% B; 2-13 min) linear increase of B from 10% to 20%; 13 -20 min) linear increase of B from 20% to 70%; 20-27 min) isocratic at 70% B; 27-29 min) linear decrease of B from 70% to 10%; 29-40 min) isocratic re-equilibration at 10% B.

The parameters of the HESI interface and of the ion optics of the Q-Exactive spectrometer were set as follows: sheath gas flow rate) 40 a.u.; auxiliary gas flow rate) 15 a.u.; spray voltage) −3 kV; capillary temperature) 200 °C; S-lens RF level 60. The mass spectrometer was operated at its maximum resolving power (140000 at *m*/*z* 200) for both full scan MS and MS/MS experiments. Full scan high-resolution MS spectra were acquired in a 300-700 *m*/*z* interval. Here, the Automatic Gain Control (AGC) level was set to 1 × 10^6, with a maximum injection time of 100 ms. A normalized collision energy (NCE) of 60 units was adopted for MS/MS experiments, while the AGC level was set

 doi:10.20944/preprints202307.1535.v1

to 2 × 10^5, with a maximum injection time of 100 ms. The spectrometer was calibrated daily by infusing, at a 5 μL/min flow rate, calibration solutions provided by the instrument manufacturer for negative polarity acquisitions. As a result, a mass accuracy always better than 5 ppm was achieved.

3.3.5. Extraction of BSE from LDH-BSE and LDHc-BSE composites

The lyophilized BSE exhibited an excellent solubility in methanol (MeOH). Hence, this solvent was initially selected as the extraction medium for the recovery of BSE in the LDH-BSE and LDHc-BSE composites. To such purpose, the inorganic-organic composite was dispersed in pure MeOH to a nominal concentration of 1 mg/mL. The mixture was vigorously stirred (1 min) using a vortex mixer and the extraction of the organic material was further supported by a further sonication step for 10 min. A DU-32 ultrasonic bath (Argo Lab, Carpi, Italy), operating at 40 KHz frequency, 120 W power and 25 °C temperature was adopted for the latter purpose. Thenceforth, the separation between the solid phase and the extraction medium was obtained after centrifugation (4500 *g*) for 10 min. The supernatant was withdrawn and diluted by a 1:10 factor in pure methanol to an overall volume of 1 mL. The sample was spiked with 50 μL of a 52.5 μg/mL methanolic solution of oleic acid (internal standard) prior to the RPLC-ESI(-)-FTMS analysis.

As proven by the FT-IR/ATR analysis of the composites before and after the extraction step (see **Section 2.3**), this extraction procedure was efficient in determining the quantitative recovery of BSE from LDH-BSE composites. Conversely, the BSE content was only partially extracted in the case of LDHc-BSE systems. To increase the extraction yield for the latter composites, we decided to adopt an alternative extraction procedure based on the acidic pretreatment of the matrix. Indeed, LDHc was proven to be quantitatively solubilized in an aqueous hydrochloric acid (HCl) solution at pH 1.2. Hence, we dispersed the LDHc-BSE in the same acidic aqueous medium to a nominal concentration of 1 mg/mL. The heterogeneous mixture was vigorously stirred for 1 min using a vortex mixer. Thereafter, pure chloroform was added in a 1:1 volume ratio in respect to the acidic aqueous phase. The mixture was stirred again for 1 min and a clear phase separation was obtained after centrifugation (4500 *g*) for 10 min. 1 mL of the organic phase was recovered and subjected to solvent evaporation under nitrogen flow. The dry residue was redissolved in 1 mL of pure MeOH. The resulting mixture was diluted by a 1:10 factor in pure methanol to an overall volume of 1 mL. Also in this case, the sample was spiked with 50 μL of a 52.5 μg/mL methanolic solution of oleic acid (internal standard) prior to the RPLC-ESI(-)-FTMS analysis.

3.3.6. Quantification of boswellic acids in LDH-BSE and LDHc-BSE composites

Two analytical strategies were adopted to assess the extent of the loading of BA in LDH-BSE and LDHc-BSE composites.

The first was based on the construction of calibration curves for α-BA, β-BA, α-ABA, β-ABA, and their isomers, starting from consecutive dilutions of a 1 mg/mL methanolic solution of lyophilized BSE. Specifically, 1 mL of the following calibration levels were obtained: Level 1 (0.1 μg/mL), Level 2 (1 μg/mL), Level 3 (5 μg/mL), Level 4 (10 μg/mL), Level 5 (50 μg/mL) and Level 6 (100 μg/mL). Each of the calibration solutions was spiked with 50 μL of a 52.5 μg/mL methanolic solution of oleic acid (ISTD) prior to the RPLC-ESI(-)-FTMS analysis. As shown in **Section 3.3.5**, the extraction procedure involved the dispersion of the composites in the extraction medium to a nominal concentration of 1 mg/mL. At the end of the process, the extracts were diluted by a 1:10 factor. Hence, the BA content of the diluted extract can be considered as representative for 100 μg of organic-inorganic composite. On the other hand, the BA amount in the upper calibration level (Level 6) is representative for the BA content in the same mass of BSE. Therefore, for each of the analytes of interest, the result of the interpolation of the analytical response (ISTD-normalized EIC areas) with the calibration curve, can be interpreted as follows: it represents the loaded amount of a BA in a given mass of the composite, expressed as the percentage of the content of that BA in the same mass of BSE.

The second quantitative approach aimed to the determination of the absolute amount of α-BA and β-BA in BSE as well as in the composites. To such purpose, an external calibration approach was adopted. Five calibration levels, corresponding to equimolar mixtures of α-BA and β-BA were

 doi:10.20944/preprints202307.1535.v1

prepared: Level 1 (0.1 μg/mL), Level 2 (1 μg/mL), Level 3 (5 μg/mL), Level 4 (10 μg/mL), Level 5 (50 μg/mL). 1 mL of each of the calibration level was spiked with 50 μL of a 52.5 μg/mL methanolic solution of oleic acid (ISTD) prior to the RPLC-ESI(-)-FTMS analysis. The calibration curves were exploited to determine the absolute amount of α-BA and β-BA in a 100 μg/mL methanolic solution of a BSE, as well as in the BSE extracts obtained from LDH/LDHc-BSE composites (see **Section 3.3.5**).

3.4. Antibacterial evaluation

The antibacterial activity of BSE, LDH, LDH-BSE, LDHc and LDHc-BSE systems against two Gram + (*Staphyloccocus aureus* ATCC 43300 and *S. epidermidis* ATCC 51625; American type culture collection – ATCC) and two Gram – pathogenic bacterial strains (*Escherichia coli* ATCC 25922 and *Pseudomonas aeruginosa* ATCC 15422) was evaluated by direct contact between bacterial strains and the composites. According to Dianhai et al., [39] reporting the concentration of 100 μg/mL as the minimum inhibitory concentration (MIC) of BSE, 1 mL of bacterial suspensions at concentration 1×10^5 CFU/mL were directly exposed to the above mentioned amount of the composites. Then, specimens were incubated in an incubator with controlled humidity and temperature (95% and 37 °C, respectively) for 24 hours. Afterwards, the number of viable bacteria was evaluated by the colonies forming unit (CFU) count as previously detailed by the Authors [50,51].

3.5. Anti-inflammatory efficacy

The composites' ability to act as antioxidant by scavenger activity was evaluated regarding their ability to preserve cells from intracellular accumulation of toxic active species in a pro-inflammatory scenario. Accordingly, oxidative stress was chemically induced by adding hydrogen peroxide (H_2O_2, 3 hours/day, 300 μM) into the medium to generate oxygen-derived toxic active species (ROS) as previously shown by the authors [43–45]. Accordingly, H_2O_2 was added to the medium in the presence of the composites and agitated (100 rpm) at room temperature for 3 days. Afterwards, 1 mL of this solution was added to a new 24-multi well plate containing human bone-marrow mesenchymal stem cells (hBMSC, $2x10^4$ cells/well, from PromoCell C-12974) and incubated at 37°C for 24 h. To verify intracellular ROS internalization, the specific CellRox reagent (CellROX ™ Deep Red Reagent kit, from Thermo Fisher Scientific, Milan, Italy) was applied and cells were further co-stained with phalloidin (Alexa Fluor 488 Phalloidin, from Thermo Fisher Scientific, Milan, Italy) to visualize cytoskeleton F-actin filaments. Images were collected by confocal microscope (Leica TCS SP8 LIGHTNING confocal laser scanning microscope). Finally, to quantify the ROS amount, the CellRox fluorescent signals (expressed as relative fluorescent unit – RFU) were detected at 640 nm and 665 nm for excitation and emission wavelengths, respectively. Cells cultivated in a regular medium with H_2O_2 were considered as control to rank the results from specimens.

3.6. Statistical data analysis

Experiments were performed using six replicates for each assay. Results were statistically analyzed using the SPSS software (v.20.0, IBM, USA). First, data normal distribution and homogeneity of variance were confirmed by the Shapiro-Wilk's and the Levene's test, respectively; then, groups were compared by the one-way ANOVA using the Tukey's test as post-hoc analysis. Significant differences were established at $p < 0.05$.

4. Conclusions

A lamellar solid layered double hydroxide (LDH), corresponding to a synthetic magnesium aluminum carbonate, was evaluated, as such or after calcination (LDHc), for its potential as a carrier of bioactive compounds included in *Boswellia Serrata* extract, poorly soluble in water. Data obtained by TGA, PXRD, FT-IR/ATR and XPS consistently suggested a disruption of the original LDH structure upon calcination. An increase in the amount of BSE-related compounds, especially α- and β-boswellic acids and the corresponding acetylated derivatives, embedded into the inorganic material was also evidenced by LC-MS analyses when LDHc was adopted. On the other hand, *in vitro* tests of

the antibacterial and anti-inflammatory activity exerted by LDH(c)-BSE composites indicated a better performance when LDH was adopted, with significant improvements with respect to BSE as such. These results suggest that anionic forms of compounds occurring in BSE were more retained in LDHc, likely due to their role as substituents of the carbonate anions originally included in the material structure, as also confirmed by FT-IR and XPS. This feature limited their subsequent release in the aqueous environment adopted for tests of biological activity. Based on these outcomes, this study opens interesting perspectives for the development of composites including LDH as deliverers of BSE bioactive compounds, exhibiting interesting combination of chemical, physical and biological properties when compared to those of the bare extract.

Supplementary Materials: The following supporting information can be downloaded at the website of this paper posted on Preprints.org.

Author Contributions: Conceptualization, S.C. and E.D.G.; methodology, S.C., F.B., A.C.1, Z.N., and R.R.; investigation, S.C., F.B., A.C.1, Z.N., and R.R.; data curation, S.C., F.B., A.C.1, Z.N., and R.R.; writing—original draft preparation, S.C., A.C.1, Z.N. and R.R.; writing—review and editing, S.C., A.C.2, I.L. and E.D.G.; supervision, E.D.G.; funding acquisition, A.C.2, I.L. and E.D.G.. All authors have read and agreed to the published version of the manuscript.

Funding: This research received no external funding.

Data Availability Statement: The data presented in this study are available herein.

Acknowledgments: Authors would thank Dr Giuseppe Iannaccone (Jaber Innovation S.r.l.) for the valuable discussions.

Conflicts of Interest: The authors declare no conflict of interest.

Sample Availability: Samples of the natural extracts, standard compounds and composites are available from the authors.

References

1. Ammon, H. Boswellic Acids in Chronic Inflammatory Diseases. *Planta Med.* **2006**, *72*, 1100–1116, doi:10.1055/s-2006-947227.
2. Iram, F.; Khan, S.A.; Husain, A. Phytochemistry and Potential Therapeutic Actions of Boswellic Acids: A Mini-Review. *Asian Pac. J. Trop. Biomed.* **2017**, *7*, 513–523, doi:10.1016/j.apjtb.2017.05.001.
3. Jaroš, P.; Timkina, E.; Michailidu, J.; Maršík, D.; Kulišová, M.; Kolouchová, I.; Demnerová, K. Boswellic Acids as Effective Antibacterial Antibiofilm Agents. *Molecules* **2022**, *27*, 3795, doi:10.3390/molecules27123795.
4. Gupta, M.; Verma, S.K.; Singh, S.; Trivedi, L.; Rout, P.K.; Vasudev, P.G.; Luqman, S.; Darokar, M.P.; Bhakuni, R.S.; Misra, L. Anti-Proliferative and Antibacterial Activity of Oleo-Gum-Resin of Boswellia Serrata Extract and Its Isolate 3-Hydroxy-11-Keto-β-Boswellic Acid. *J. Herb. Med.* **2022**, *32*, 100546, doi:10.1016/j.hermed.2022.100546.
5. Sharma, A.; Gupta, N.K.; Dixit, V.K. Complexation with Phosphatidyl Choline as a Strategy for Absorption Enhancement of Boswellic Acid. *Drug Deliv.* **2010**, *17*, 587–595, doi:10.3109/10717544.2010.501461.
6. Hüsch, J.; Bohnet, J.; Fricker, G.; Skarke, C.; Artaria, C.; Appendino, G.; Schubert-Zsilavecz, M.; Abdel-Tawab, M. Enhanced Absorption of Boswellic Acids by a Lecithin Delivery Form (Phytosome®) of Boswellia Extract. *Fitoterapia* **2013**, *84*, 89–98, doi:10.1016/j.fitote.2012.10.002.
7. Hüsch, J.; Gerbeth, K.; Fricker, G.; Setzer, C.; Zirkel, J.; Rebmann, H.; Schubert-Zsilavecz, M.; Abdel-Tawab, M. Effect of Phospholipid-Based Formulations of Boswellia Serrata Extract on the Solubility, Permeability, and Absorption of the Individual Boswellic Acid Constituents Present. *J. Nat. Prod.* **2012**, *75*, 1675–1682, doi:10.1021/np300009w.
8. Tambe, A.; Pandita, N.; Kharkar, P.; Sahu, N. Encapsulation of Boswellic Acid with β- and Hydroxypropyl-β-Cyclodextrin: Synthesis, Characterization, in Vitro Drug Release and Molecular Modelling Studies. *J. Mol. Struct.* **2018**, *1154*, 504–510, doi:10.1016/j.molstruc.2017.10.061.
9. Mehta, M.; Dureja, H.; Garg, M. Development and Optimization of Boswellic Acid-Loaded Proniosomal Gel. *Drug Deliv.* **2016**, *23*, 3072–3081, doi:10.3109/10717544.2016.1149744.
10. Solanki, N.; Mehta, M.; Chellappan, D.K.; Gupta, G.; Hansbro, N.G.; Tambuwala, M.M.; AA Aljabali, A.; Paudel, K.R.; Liu, G.; Satija, S.; et al. Antiproliferative Effects of Boswellic Acid-Loaded Chitosan

Nanoparticles on Human Lung Cancer Cell Line A549. *Future Med. Chem.* **2020**, *12*, 2019–2034, doi:10.4155/fmc-2020-0083.

11. AGUZZI, C.; CEREZO, P.; VISERAS, C.; CARAMELLA, C. Use of Clays as Drug Delivery Systems: Possibilities and Limitations. *Appl. Clay Sci.* **2007**, *36*, 22–36, doi:10.1016/j.clay.2006.06.015.
12. Rodrigues, L.A. de S.; Figueiras, A.; Veiga, F.; de Freitas, R.M.; Nunes, L.C.C.; da Silva Filho, E.C.; da Silva Leite, C.M. The Systems Containing Clays and Clay Minerals from Modified Drug Release: A Review. *Colloids Surfaces B Biointerfaces* **2013**, *103*, 642–651, doi:10.1016/j.colsurfb.2012.10.068.
13. Dong, J.; Cheng, Z.; Tan, S.; Zhu, Q. Clay Nanoparticles as Pharmaceutical Carriers in Drug Delivery Systems. *Expert Opin. Drug Deliv.* **2021**, *18*, 695–714, doi:10.1080/17425247.2021.1862792.
14. Costantino, U.; Ambrogi, V.; Nocchetti, M.; Perioli, L. Hydrotalcite-like Compounds: Versatile Layered Hosts of Molecular Anions with Biological Activity. *Microporous Mesoporous Mater.* **2008**, *107*, 149–160, doi:10.1016/j.micromeso.2007.02.005.
15. Kankala, R.K. Nanoarchitectured Two-Dimensional Layered Double Hydroxides-Based Nanocomposites for Biomedical Applications. *Adv. Drug Deliv. Rev.* **2022**, *186*, 114270, doi:10.1016/j.addr.2022.114270.
16. Choi, S.-J.; Oh, J.-M.; Choy, J.-H. Toxicological Effects of Inorganic Nanoparticles on Human Lung Cancer A549 Cells. *J. Inorg. Biochem.* **2009**, *103*, 463–471, doi:10.1016/j.jinorgbio.2008.12.017.
17. Haraketi, M.; Hosni, K.; Srasra, E. Intercalation Behavior of Salicylic Acid into Calcined Cu-Al-Layered Double Hydroxides for a Controlled Release Formulation. *Surf. Eng. Appl. Electrochem.* **2017**, *53*, 360–370, doi:10.3103/S106837551704007X.
18. Ambrogi, V.; Fardella, G.; Grandolini, G.; Nocchetti, M.; Perioli, L. Effect of Hydrotalcite-like Compounds on the Aqueous Solubility of Some Poorly Water-Soluble Drugs. *J. Pharm. Sci.* **2003**, *92*, 1407–1418, doi:10.1002/jps.10411.
19. Del Arco, M.; Fernández, A.; Martín, C.; Sayalero, M.L.; Rives, V. Solubility and Release of Fenamates Intercalated in Layered Double Hydroxides. *Clay Miner.* **2008**, *43*, 255–265, doi:10.1180/claymin.2008.043.2.08.
20. Bi, X.; Zhang, H.; Dou, L. Layered Double Hydroxide-Based Nanocarriers for Drug Delivery. *Pharmaceutics* **2014**, *6*, 298–332, doi:10.3390/pharmaceutics6020298.
21. Bernard, E.; Zucha, W.J.; Lothenbach, B.; Mäder, U. Stability of Hydrotalcite (Mg-Al Layered Double Hydroxide) in Presence of Different Anions. *Cem. Concr. Res.* **2022**, *152*, 106674, doi:10.1016/j.cemconres.2021.106674.
22. Stanimirova, T.; Piperov, N.; Petrova, N.; Kirov, G. Thermal Evolution of Mg-Al-CO 3 Hydrotalcites. *Clay Miner.* **2004**, *39*, 177–191, doi:10.1180/0009855043920129.
23. Allmann, R.J.; Neues, H.P. Die Struktur Des Hydrotalkits. *Jahrb. für Mineral. Monatshefte* **1969**, 544–551.
24. Del Arco, M.; Cebadera, E.; Gutiérrez, S.; Martín, C.; Montero, M.J.; Rives, V.; Rocha, J.; Sevilla, M.A. Mg,Al Layered Double Hydroxides with Intercalated Indomethacin: Synthesis, Characterization, and Pharmacological Study. *J. Pharm. Sci.* **2004**, *93*, 1649–1658, doi:10.1002/jps.20054.
25. Rocha, J.; del Arco, M.; Rives, V.; Ulibarri, M.A. Reconstruction of Layered Double Hydroxides from Calcined Precursors: A Powder XRD and 27Al MAS NMR Study. *J. Mater. Chem.* **1999**, *9*, 2499–2503, doi:10.1039/a903231b.
26. San Román, M.S.; Holgado, M.J.; Salinas, B.; Rives, V. Characterisation of Diclofenac, Ketoprofen or Chloramphenicol Succinate Encapsulated in Layered Double Hydroxides with the Hydrotalcite-Type Structure. *Appl. Clay Sci.* **2012**, *55*, 158–163, doi:10.1016/j.clay.2011.11.010.
27. Yin, H.; Cui, L.; Ai, S.; Fan, H.; Zhu, L. Electrochemical Determination of Bisphenol A at Mg–Al–CO3 Layered Double Hydroxide Modified Glassy Carbon Electrode. *Electrochim. Acta* **2010**, *55*, 603–610, doi:10.1016/j.electacta.2009.09.020.
28. Mališová, M.; Horňáček, M.; Mikulec, J.; Hudec, P.; Jorík, V. FTIR Study of Hydrotalcite. *Acta Chim. Slovaca* **2018**, *11*, 147–156, doi:10.2478/acs-2018-0021.
29. De Giglio, E.; Ditaranto, N.; Sabbatini, L. Polymer Surface Chemistry: Characterization by XPS. In *Polymer Surface Characterization*; De Gruyter, 2022; pp. 45–88.
30. Zhang, C.; Sun, L.; Tian, R.; Jin, H.; Ma, S.; Gu, B. Combination of Quantitative Analysis and Chemometric Analysis for the Quality Evaluation of Three Different Frankincenses by Ultra High Performance Liquid Chromatography and Quadrupole Time of Flight Mass Spectrometry. *J. Sep. Sci.* **2015**, *38*, 3324–3330, doi:10.1002/jssc.201500326.
31. Shah, B.A.; Qazi, G.N.; Taneja, S.C. Boswellic Acids: A Group of Medicinally Important Compounds. *Nat.*

Prod. Rep. **2009**, *26*, 72–89, doi:10.1039/B809437N.

32. Börner, F.; Werner, M.; Ertelt, J.; Meins, J.; Abdel-Tawab, M.; Werz, O. Analysis of Boswellic Acid Contents and Related Pharmacological Activities of Frankincense-Based Remedies That Modulate Inflammation. *Pharmaceuticals* **2021**, *14*, 660, doi:10.3390/ph14070660.
33. Schmiech, M.; Lang, S.J.; Werner, K.; Rashan, L.J.; Syrovets, T.; Simmet, T. Comparative Analysis of Pentacyclic Triterpenic Acid Compositions in Oleogum Resins of Different Boswellia Species and Their In Vitro Cytotoxicity against Treatment-Resistant Human Breast Cancer Cells. *Molecules* **2019**, *24*, 2153, doi:10.3390/molecules24112153.
34. Zhang, Y.; Ning, Z.; Lu, C.; Zhao, S.; Wang, J.; Liu, B.; Xu, X.; Liu, Y. Triterpenoid Resinous Metabolites from the Genus Boswellia: Pharmacological Activities and Potential Species-Identifying Properties. *Chem. Cent. J.* **2013**, *7*, 153, doi:10.1186/1752-153X-7-153.
35. Schmiech, M.; Ulrich, J.; Lang, S.J.; Büchele, B.; Paetz, C.; St-Gelais, A.; Syrovets, T.; Simmet, T. 11-Keto-α-Boswellic Acid, a Novel Triterpenoid from Boswellia Spp. with Chemotaxonomic Potential and Antitumor Activity against Triple-Negative Breast Cancer Cells. *Molecules* **2021**, *26*, 366, doi:10.3390/molecules26020366.
36. Asteggiano, A.; Curatolo, L.; Schiavo, V.; Occhipinti, A.; Medana, C. Development, Validation, and Application of a Simple and Rugged HPLC Method for Boswellic Acids for a Comparative Study of Their Abundance in Different Species of Boswellia Gum Resins. *Appl. Sci.* **2023**, *13*, 1254, doi:10.3390/app13031254.
37. Sharma, A.; Biharee, A.; Kumar, A.; Jaitak, V. Antimicrobial Terpenoids as a Potential Substitute in Overcoming Antimicrobial Resistance. *Curr. Drug Targets* **2020**, *21*, 1476–1494, doi:10.2174/1389450121666200520103427.
38. Chourmouziadi Laleni, N.; Gomes, P.D.C.; Gkatzionis, K.; Spyropoulos, F. Propolis Particles Incorporated in Aqueous Formulations with Enhanced Antibacterial Performance. *Food Hydrocoll. Heal.* **2021**, *1*, 100040, doi:10.1016/j.fhfh.2021.100040.
39. Bi, D.; Chen, G.; Cheng, J.; Wen, J.; Pei, N.; Zeng, H.; Li, Y. Boswellic Acid Captivated Hydroxyapatite Carboxymethyl Cellulose Composites for the Enhancement of Chondrocytes in Cartilage Repair. *Arab. J. Chem.* **2020**, *13*, 5605–5613, doi:10.1016/j.arabjc.2020.03.030.
40. Narasagoudr, S.S.; Hegde, V.G.; Chougale, R.B.; Masti, S.P.; Dixit, S. Influence of Boswellic Acid on Multifunctional Properties of Chitosan/Poly (Vinyl Alcohol) Films for Active Food Packaging. *Int. J. Biol. Macromol.* **2020**, *154*, 48–61, doi:10.1016/j.ijbiomac.2020.03.073.
41. Poeckel, D.; Werz, O. Boswellic Acids: Biological Actions and Molecular Targets. *Curr. Med. Chem.* **2006**, *13*, 3359–3369, doi:10.2174/092986706779010333.
42. Bharti, A.C.; Donato, N.; Singh, S.; Aggarwal, B.B. Curcumin (Diferuloylmethane) down-Regulates the Constitutive Activation of Nuclear Factor–KB and IκBα Kinase in Human Multiple Myeloma Cells, Leading to Suppression of Proliferation and Induction of Apoptosis. *Blood* **2003**, *101*, 1053–1062, doi:10.1182/blood-2002-05-1320.
43. Gamna, F.; Yamaguchi, S.; Cochis, A.; Ferraris, S.; Kumar, A.; Rimondini, L.; Spriano, S. Conferring Antioxidant Activity to an Antibacterial and Bioactive Titanium Surface through the Grafting of a Natural Extract. *Nanomaterials* **2023**, *13*, 479, doi:10.3390/nano13030479.
44. Bonifacio, M.A.; Cochis, A.; Cometa, S.; Gentile, P.; Scalzone, A.; Scalia, A.C.; Rimondini, L.; De Giglio, E. From the Sea to the Bee: Gellan Gum-Honey-Diatom Composite to Deliver Resveratrol for Cartilage Regeneration under Oxidative Stress Conditions. *Carbohydr. Polym.* **2020**, *245*, 116410, doi:10.1016/j.carbpol.2020.116410.
45. Alfieri, M.L.; Riccucci, G.; Ferraris, S.; Cochis, A.; Scalia, A.C.; Rimondini, L.; Panzella, L.; Spriano, S.; Napolitano, A. Deposition of Antioxidant and Cytocompatible Caffeic Acid-Based Thin Films onto Ti6Al4V Alloys through Hexamethylenediamine-Mediated Crosslinking. *ACS Appl. Mater. Interfaces* **2023**, *15*, 29618–29635, doi:10.1021/acsami.3c05564.
46. Börner, F.; Pace, S.; Jordan, P.M.; Gerstmeier, J.; Gomez, M.; Rossi, A.; Gilbert, N.C.; Newcomer, M.E.; Werz, O. Allosteric Activation of 15-Lipoxygenase-1 by Boswellic Acid Induces the Lipid Mediator Class Switch to Promote Resolution of Inflammation. *Adv. Sci.* **2023**, *10*, 2205604, doi:10.1002/advs.202205604.
47. Siddhu, N.S.S.; Guru, A.; Satish Kumar, R.C.; Almutairi, B.O.; Almutairi, M.H.; Juliet, A.; Vijayakumar, T.M.; Arockiaraj, J. Pro-Inflammatory Cytokine Molecules from Boswellia Serrate Suppresses Lipopolysaccharides Induced Inflammation Demonstrated in an in-Vivo Zebrafish Larval Model. *Mol. Biol.*

Rep. **2022**, *49*, 7425–7435, doi:10.1007/s11033-022-07544-5.

48. Miyata, S. Anion-Exchange Properties of Hydrotalcite-Like Compounds. *Clays Clay Miner.* **1983**, *31*, 305–311, doi:10.1346/CCMN.1983.0310409.
49. Parker, L.M.; Milestone, N.B.; Newman, R.H. The Use of Hydrotalcite as an Anion Absorbent. *Ind. Eng. Chem. Res.* **1995**, *34*, 1196–1202, doi:10.1021/ie00043a023.
50. Cochis, A.; Azzimonti, B.; Della Valle, C.; De Giglio, E.; Bloise, N.; Visai, L.; Cometa, S.; Rimondini, L.; Chiesa, R. The Effect of Silver or Gallium Doped Titanium against the Multidrug Resistant Acinetobacter Baumannii. *Biomaterials* **2016**, *80*, 80–95, doi:10.1016/j.biomaterials.2015.11.042.
51. Ferraris, S.; Cochis, A.; Cazzola, M.; Tortello, M.; Scalia, A.; Spriano, S.; Rimondini, L. Cytocompatible and Anti-Bacterial Adhesion Nanotextured Titanium Oxide Layer on Titanium Surfaces for Dental and Orthopedic Implants. *Front. Bioeng. Biotechnol.* **2019**, *7*, doi:10.3389/fbioe.2019.00103.